Overview of Mars surface geochemical diversity through Alpha Particle X-Ray Spectrometer data multidimensional analysis: First attempt at modeling rock alteration

Erwan Tréguier,[1] Claude d'Uston,[1] Patrick C. Pinet,[2] Gilles Berger,[3] Michael J. Toplis,[2] Timothy J. McCoy,[4] Ralf Gellert,[5] and Johannes Brückner[6]

Received 4 October 2007; revised 4 March 2008; accepted 31 July 2008; published 6 November 2008.

[1] Principal component analysis and a hierarchical clustering method have been employed to describe and quantify the compositional variability of Martian rocks and soils measured by the Alpha Particle X-Ray Spectrometers onboard the Mars Exploration Rovers. A robust classification of samples emerges which defines distinct rock classes and sheds light on the petrogenetic relationships between rocks. This is particularly useful in the case of rocks from Gusev Crater, where significant chemical diversity is observed. This approach also highlights that compositional variability of rocks at Meridiani is dominated by variations in sulfur content; the relative proportions of other elements remaining approximately constant. For soils, variations in Fe concentration dominate because of the presence of hematite-rich ''berry''-bearing samples. On the basis of this observation, a simple geochemical model of acid fog alteration of Martian basalts has been tested, assuming either equivalent alteration of all phases or preferential alteration of certain phases (thus taking into account kinetic considerations). The results show that for certain ranges of SO_3/basalt, many of the compositional and mineralogical features measured at both sites may be explained. The secondary mineralogy and bulk rock compositions predicted by the model are broadly consistent with rock and soil compositions from Gusev and Meridiani, especially if the role of brine circulation and evaporation are considered. Although agreement is not perfect, comparison of observations and models argues in favor of variable interaction of the Martian surface with sour gas, explaining the high local abundance of sulfates, for example.

Citation: Tréguier, E., C. d'Uston, P. C. Pinet, G. Berger, M. J. Toplis, T. J. McCoy, R. Gellert, and J. Brückner (2008), Overview of Mars surface geochemical diversity through Alpha Particle X-Ray Spectrometer data multidimensional analysis: First attempt at modeling rock alteration, *J. Geophys. Res.*, *113*, E12S34, doi:10.1029/2007JE003010.

1. Introduction

[2] Since January 2004, the twin rovers Spirit and Opportunity of the Mars Exploration Rover (MER) mission have been investigating their respective landing sites at Gusev Crater and Meridiani Planum thanks to the Athena Science Payload [*Squyres et al.*, 2003]. This scientific payload includes the Alpha Particle X-Ray Spectrometer (APXS) [*Rieder et al.*, 2003] whose role is to determine the elemental composition of the material found at the Martian surface. Because of their intrinsic mobility and their extraordinary longevity, Spirit and Opportunity have been able to reach distances several kilometers from their landing sites. Along the way, the complementary suite of instruments onboard the two rovers has characterized diverse geological sites [*Arvidson et al.*, 2006a; *Squyres et al.*, 2006a, 2006b], leading to an enormous increase in our knowledge and understanding of the Martian surface. After 1260 sols, the two APXS instruments have analyzed approximately 300 soils and rocks (Table 1). Chemical composition data are found in the works by *Gellert et al.* [2004], *Rieder et al.* [2004], *Brückner et al.* [2006], and *Gellert et al.* [2006]. It is the aim of the work presented here to extend our understanding of the geochemical relationships among these samples using numerical multidimensional analysis techniques such as principal component analysis (PCA) [*Murtagh and Heck*, 1987]. The unsupervised classification successfully performed on abraded rocks of Gusev [*Tréguier et al.*, 2006] is extended here to other types of samples at both sites, including the most recent data. The results of the PCA on several subsets of samples are also

[1]Centre d'Etude Spatiale des Rayonnements, OMP, Université Paul Sabatier, CNRS, Toulouse, France.
[2]Dynamique Terrestre et Planétaire, OMP, Université Paul Sabatier, CNRS, Toulouse, France.
[3]Laboratoire d'étude des Mécanismes de Transfert en Géologie, OMP, Université Paul Sabatier, CNRS, Toulouse, France.
[4]Department of Mineral Sciences, National Museum of Natural History, Smithsonian Institution, Washington, D. C., USA.
[5]Department of Physics, University of Guelph, Guelph, Ontario, Canada.
[6]Max-Planck-Institut für Chemie, Mainz, Germany.

0148-0227/08/2007JE003010

Table 1. Number of Alpha Particle X-Ray Spectrometer Measurements by Site and Kind of Target[a]

	Gusev	Meridiani
Undisturbed rocks (RU)	50	40
Brushed rocks (RB)	44	15
RATed rocks (RR)	15	31
RAT fines (RF)	1	0
Undisturbed soils (SU)	30	25
Disturbed soils (SD)	26	6
Trench soils (ST)	6	6
Soil clods (SC)	3	0
All samples	175	123

[a]Until sol 1260 for both rovers, counting Heat Shield Rock measurements.

analyzed using a hierarchical clustering method [*Kaufman and Rousseeuw*, 1990] in order to define statistically significant clusters. First of all, the whole data set is considered in order to provide an overview of the global geochemical diversity observed by the rovers, before focusing on each individual landing site. Although PCA is a purely statistical method, the results obtained highlight geochemical trends which may be interpreted in terms of the physical and chemical processes responsible for the creation of compositional diversity. With this idea in mind, the PC analyses have been combined with available mineralogical data and the results of numerical simulations of basalt alteration. In this way it is possible to constrain the conditions prevailing during interaction between pristine magmatic rocks and the Martian atmosphere.

2. Data Set and Multidimensional Method

2.1. APXS Data Set

[3] Table 1 presents the number of APXS measurements, sorted by kind of target, for each landing site (note that this list includes neither calibration nor magnet measurements). The samples have been arranged in eight different categories: four for the rocks and four for the soils. Thanks to the Rock Abrasion Tool (RAT) it is not only possible to measure undisturbed rock surfaces (RU) as was the case for Mars Pathfinder, but also brushed (RB) and abraded (RR) surfaces [*Gorevan et al.*, 2003]. An additional category, including only one sample at the present time, is RAT fines (RF). The samples listed as soils are loose, unconsolidated materials that can be distinguished from rocks, bedrock, or strongly cohesive sediments [*Squyres et al.*, 2004]. The soils are divided into the categories, undisturbed soils (SU), disturbed soils (SD), trenches (ST), and soil clods (SC). A total of 298 samples have been analyzed until sol 1260 (for both rovers).

[4] The APXS instrument usually gives estimates of the weight abundances of 16 chemical elements: Na, Mg, Al, Si, P, S, Cl, K, Ca, Ti, Cr, Mn, Fe, Ni, Zn, and Br. Although some other trace elements are occasionally detected (Co, Cu, Ga, Ge, Rb, Sr, Y, Ba, and Pb) [*Yen et al.*, 2006], they are not considered in our study. For each measured element i, accuracy depends only on the instrument and is defined by a standard deviation λ_i. Precision is specific to each single measurement j and is defined by a standard deviation $\mu_{i,j}$. Thus, the total uncertainty, for each element i and each measurement j, is defined by a standard deviation $\sigma_{i,j}$, being the quadratic sum of accuracy and precision:

$$\sigma_{i,j} = \sqrt{\lambda_i^2 + \mu_{i,j}^2}. \quad (1)$$

[5] Before using a multidimensional method for analyzing the data, we have checked that the coefficient of variation (the ratio between the standard deviation and the mean value) for the abundances of a given element is greater than the average relative uncertainty for this element. This was checked for the different subsets of APXS data on which a PCA was performed. This test was always successful with the single exception of the subset of Meridiani RAT-abraded (RATed) samples. In this case, four elements failed: P, K, Cr, and Fe (Table 2), and for this

Table 2. Total Relative Uncertainty and Coefficient of Variation for Each Analyzed Data Set for the Abundances of the 16 Usually Measured Elements[a]

		Coefficient of Variation					
Element	Total Uncertainty	Whole Data Set	Gusev RR[b]	Gusev RB[b]	Gusev RU[b]	Meridiani RR[b]	Meridiani All Samples
Na	14.7	30.3	49.0	30.6	24.3	23.6	24.6
Mg	14.1	33.3	41.0	43.8	26.3	15.8	20.8
Al	7.3	26.7	35.4	31.3	26.4	14.2	17.1
Si	3.1	14.1	7.3	15.3	14.3	8.9	8.9
P	15.2	67.3	106.5	64.3	57.2	6.1	14.6
S	15.0	78.3	88.4	38.5	35.9	22.0	56.3
Cl	30.2	48.0	66.9	51.4	37.2	55.2	43.7
K	27.2	69.4	91.2	104.8	85.1	22.5	30.9
Ca	7.1	26.0	31.4	29.9	29.6	26.5	22.4
Ti	20.3	56.3	78.4	70.9	62.4	22.4	30.8
Cr	21.1	85.8	78.5	145.8	148.2	13.4	36.9
Mn	13.4	26.8	40.0	125.0	37.3	13.8	17.1
Fe	7.1	25.2	16.8	26.3	26.7	6.8	25.3
Ni	18.4	55.4	71.7	85.7	70.0	27.0	45.9
Zn	22.5	76.0	40.6	108.0	89.2	28.3	30.5
Br	28.4	138.0	93.6	113.8	144.1	119.5	135.4

[a]Average value of the total uncertainty is evaluated as the quadratic sum of average accuracy [*Gellert et al.*, 2006] and average precision [*Gellert et al.*, 2004]. Note that the coefficient of variation is greater than the total uncertainty for all the 16 elements. Values are expressed in percentages.
[b]Abraded surfaces, RR; brushed surfaces, RB; and undisturbed rock surfaces, RU.

subset of data only, these four elements were not taken into consideration for the PCA analysis.

[6] The iron-nickel meteorite Heat Shield Rock (HSR) encountered by Opportunity was systematically removed from the data set as its composition is highly distinct from all other samples. This choice is more than justified given that this rock is clearly of nonMartian provenance, and not representative of the geological context [*Arvidson and Squyres*, 2005]. Note that the names of rocks and soils used here have been given by the Athena Science Team but are not officially recognized by the International Astronomical Union.

2.2. Principle of PCA

[7] Even if PCA is a common tool for investigating multidimensional data, for instance in planetary remote sensing observations [e.g., *Pinet et al.*, 2000; *Chevrel et al.*, 2002], it is not frequently applied to data sets of the chemical composition of solid samples, even on Earth. Nevertheless this technique was recently chosen to identify geobiological signatures in terrestrial samples [*Storrie-Lombardi and Fisk*, 2004; *Storrie-Lombardi and Hoover*, 2004] and for investigating the chemical variability among early data of the MER mission [*Kolb et al.*, 2006]. Note that another multidimensional method, correspondence analysis, was also employed using both APXS and Mössbauer data from the MER rovers [*Arvidson et al.*, 2006a, 2006b].

[8] PCA is a mathematical technique that reduces the dimensionality of a complex system of correlations into a smaller number of dimensions accounting for a maximum of the data variance. It transforms a number of potentially correlated variables (here: the elemental abundances) into a smaller number of uncorrelated variables: the principal components (PC). The first PC accounts for as much of the data variance as possible and each successive component accounts for as much of the remaining variance as possible. A change of reference frame is then performed (from the initial basis of elemental or oxide concentrations to the new basis of the PC), which allows the data to be studied in the new component space. The PCA can be performed either on raw data or on standardized data (mean = 0 and standard deviation = 1), the second option placing greater weight on relative variations in concentration, rather than absolute values of abundance. The data may then be plotted in the new PC space, on axes which highlight the compositional variance in a way which is not necessarily apparent on simpler elemental or oxide variation diagrams. In order to assess the significance of the results, uncertainties in the new reference frame are estimated as explained in section 2.3.

2.3. Uncertainties in Principal Component Space

[9] Assuming that the total uncertainties $\sigma_{i,j}$ (see section 2.1), for the different chemical elements, are independent of each other, the law of propagation of errors can be applied for computing the uncertainties in the new space of the principal components, for each measurement j:

$$\sigma^2_{i,jnew} = \sum_{k=1}^{n} \left(\frac{\partial x_{inew}}{\partial x_{kold}} \right)^2 \sigma^2_{k,jold}, \tag{2}$$

where n is the number of considered elements, $\sigma_{k,jold}$ is the total uncertainty for the kth chemical element, $\sigma_{i,jnew}$ is the propagated uncertainty on the ith principal axis, and $\frac{\partial x_{inew}}{\partial x_{kold}}$ designates the partial derivative of the coordinate on the ith principal axis for the kth initial variable (the abundances for the kth element of our list) and evaluated for the considered point of measurement.

[10] As the studied case is linear, these derivatives are constant, having the value of the coefficients $a_{i,k}$ of the inverse transformation matrix of the PCA and consequently do not depend on the relative abundances of the considered measurement j. The propagated uncertainty is thus given by:

$$\sigma_{i,jnew} = \sqrt{\sum_{k=1}^{n} a^2_{i,k} \sigma^2_{k,jold}}. \tag{3}$$

2.4. Classification of Samples by Hierarchical Clustering

[11] Once the PCA has been performed, further mathematical tools may be used to classify samples into statistically meaningful clusters (e.g., hierarchical clustering [*Kaufman and Rousseeuw*, 1990]). Classification of samples into clusters is of interest as groups defined in this way may potentially shed light on the petrogenetic relationships between the measured samples. From a mathematical point of view, it is important to consider and to distinguish the distance between points and the distance between clusters in the relevant PC space. The point to point distance used is the Euclidian distance in the PC space (taking all the n principal components into account):

$$d(X,Y) = \sqrt{\sum_{k=1}^{n} (y_{knew} - x_{knew})^2}; \tag{4}$$

and the cluster to cluster distance used is the average linkage clustering distance (the mean distance between the points of each cluster):

$$d(A,B) = \frac{1}{card(A) \cdot card(B)} \sum_{(X,Y) \in A \times B} d(X,Y). \tag{5}$$

[12] The result of the hierarchical clustering is usually presented in the form of a dendrogram (Figures 2, 3a–3c, and 6) with the cluster to cluster distance on the x axis. An important feature of this representation is the line that allows definition of distinct clusters (the phenon line). This line must be placed at a distance sufficiently large to avoid defining spurious clusters caused by simple measurement errors. For this purpose, the maximum norm of the propagated error for each measurement among the subset of samples used for the hierarchical clustering is taken as a minimum limit. The line marking the maximum error norm and the phenon line used for defining the clusters are both represented on each dendrogram (Figures 2, 3a–3c, and 6).

3. Results of the Multidimensional Analysis

[13] The statistical method presented here is independent of considerations of the mineralogy or geological context of

Table 3. Percentage of Variance Absorbed by All the 16 Principal Components Arranged in Descending Order for the Global Analysis on Standardized Abundances

	Principle Component Index[a]															
	1	2	3	4	5	6	7	8	9	10	11	12	13	14	15	16
Variance	24.7	13.7	12.9	9.3	6.6	6.4	5.8	4.6	4.0	3.1	2.8	2.6	1.7	1.1	0.5	<0.1
Cumulative variance	24.7	38.4	51.3	60.6	67.2	73.6	79.4	84.1	88.1	91.2	94.0	96.6	98.3	99.4	99.9	100

[a]PC1 being the first principal component, PC2 the second principal component, and so on.

the samples. In this respect the PCA may be used to provide independent confirmation of the definition of groups of samples based upon geologic or petrographic criteria. Furthermore, the PCA may highlight geochemical trends not immediately obvious in more simple representations, providing potential insight into the origin and history of the analyzed rocks, and the geological history of the Martian surface in general, as discussed below.

3.1. Global Geochemical Diversity Considering Both Gusev and Meridiani

[14] In order to provide an overview of the global chemical diversity observed by the two rovers, a PCA has been performed on all the APXS samples (rock and soil measurements, except HSR) at both sites, and considering all 16 chemical elements with their standardized abundances (see section 2.2). The simultaneous consideration of data from both sites is of interest as in this way it may be assessed to what extent the rocks at the two landing sites are similar, and answer questions such as whether chemical alteration of basaltic precursors takes place in similar or distinct ways in different places.

[15] Table 3 shows how much of the variance is accounted for by each principal component and Figure 1 shows data in the PC1 versus PC2 plane. Note that this is a projection onto a plane representing 38% of total data variance: points plotting close to each other do not fully guarantee that they are geochemically similar, but points plotting far from each other guarantee that they are geochemically different. Nevertheless, Figure 1 clearly reveals a weaker chemical diversity among the soils than among the rocks. This observation is valid for the six first PC (not represented here), that are accounting for 74% of total data variance (Table 3). This is in agreement with the fact that the main constituents of the soils are very similar at the different landing sites on Mars: a bright dust component, that represents a global unit homogenized by Aeolian activity, and dark basaltic soil deposits, that could represent another global unit or be derived from similar basaltic rocks [*Yen et al.*, 2005]. Several Gusev soil samples are an exception to this rule. Most of them, like Paso Robles and Dead Sea (Figure 1), are some of the sulfate-rich soils listed by *Wang et al.* [2007]. Their origin remains uncertain but precipitations of salt-rich fluids, fumarolic processes and Aeolian processes are among the current hypotheses. Gertrude Weise, another soil sample measured recently, also appears to be very different from the majority of the soils because of its very high concentration in silicon.

[16] Among rock samples, most end-members on Figure 1 are either RATed surfaces or brushed/undisturbed surfaces encountered at Gusev after Spirit's RAT was worn out. This happened after ~15 abrasions, the last one being for sol 416 (Watchtower), while Opportunity's RAT is still in working order, but has been used sparingly in recent times in anticipation of exploration of Victoria Crater. For Gusev data acquired prior to sol 416, the measurements made on undisturbed rock surfaces (samples covered by dust) show less compositional scatter than measurements made on surfaces abraded by the RAT, for which the dust layer has been removed. As the APXS measurement probes the surface with a depth of analysis of only several tenths of a micron (the exact distance varying with atomic number), this observation may be due to the homogenizing effect of the dust and is in agreement with the idea of a globally mixed Martian dust reservoir [*Greeley et al.*, 2006]. This effect would probably be even more obvious on Figure 1 if more data on RATed surfaces were available. These observations confirm the interest of the RAT for exposing the fresh surface of the rocks, providing a much clearer picture of the true compositional diversity of Martian rocks.

[17] Subsequently to the PCA, we performed a hierarchical clustering on the subset of RATed samples. The resulting dendrogram is shown on Figure 2 (when several RATed measurements are available for different targets on the same rock, they are numbered with a superscript). This allowed us to define seven clusters: five clusters containing only Gusev samples and two clusters containing exclusively Meridiani samples (Figure 1).

[18] For the Gusev samples, it is of note that Spirit crossed basaltic plains before reaching and successfully climbing some hills named Columbia Hills [*Arvidson et al.*, 2006a]. The five Gusev clusters correspond to the five sets of rocks already identified by *Tréguier et al.* [2006], which were found to be in good agreement with previous classifications of these rocks based upon observations from various instruments of the Athena scientific payload, and

Table 4. Percentage of Variance Absorbed by All the 16 Principal Components Arranged in Descending Order for the Meridiani Analysis on Nonstandardized Abundances

	Principal Component Index[a]															
	1	2	3	4	5	6	7	8	9	10	11	12	13	14	15	16
Variance	66.4	25.3	5.6	1.2	0.9	0.3	0.2	<0.1	<0.1	<0.1	<0.1	<0.1	<0.1	<0.1	<0.1	<0.1
Cumulative variance	66.4	91.7	97.3	98.5	99.4	99.7	99.9	99.9	100	100	100	100	100	100	100	100

[a]PC1 being the first principal component, PC2 the second principal component, and so on.

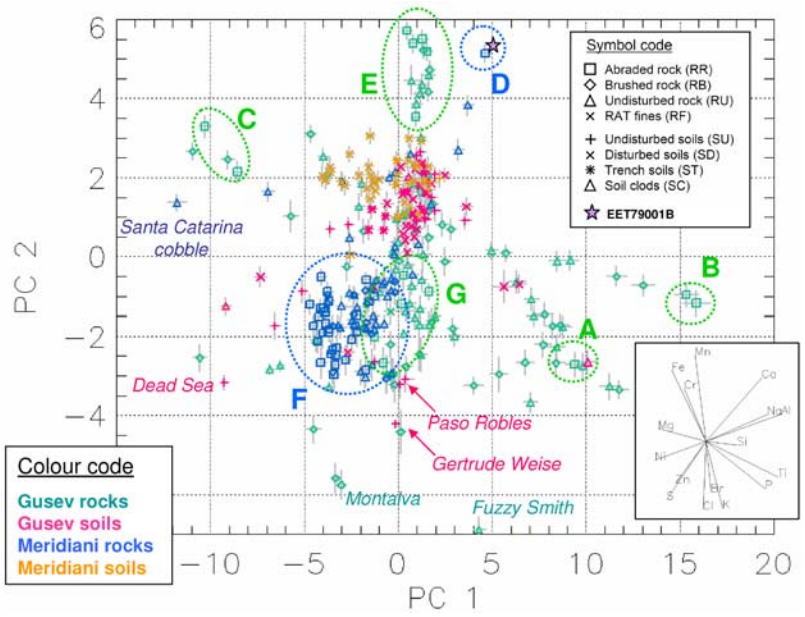

Figure 1. Scatterplot of the measurement points in the plane of the first two principal axes of the PC space for the principal component analysis (PCA) performed on the whole set of samples from both sites with standardized elemental weight abundances. Clusters identified through hierarchical clustering among RATed samples are identified with the same label as on Figure 2.

interpreted to reflect different geological units [*Squyres et al.*, 2006a; *Arvidson et al.*, 2006a; *Ming et al.*, 2006]. In the next part of this paper, we will use the term "cluster" when referring to sets of samples identified thanks to the hierarchical clustering and the term "class" when referring to sets of rocks determined by *Squyres et al.* [2006a], *Arvidson et al.* [2006a], and *Ming et al.* [2006]. We summarize here the coherence of our clusters with the geologically defined classes.

[19] The basaltic rocks of the plains (Adirondack class rocks) have been described to be rather homogeneous in composition, showing much less geochemical diversity than rocks encountered in the Columbia Hills. This is confirmed by our analysis, for which the basaltic rocks form a clearly distinct cluster (cluster E on Figures 1 and 2). These olivine-rich basalts, encountered in the plains of Gusev, are similar to certain Martian meteorites (olivine-phyric Shergottites) [*McSween et al.*, 2006a]. This can be seen on Figure 1, where the composition of the olivine-phyric Shergottite EET79001 (lithology B), taken from *Lodders* [1998], has been converted into the PC space (without being used for the definition of the principal components) and plotted in the PC1 versus PC2 plane. EET79001 is also very similar to a singular rock in Meridiani, called Bounce, as described below. Geologically it has been suggested that the rocks of the plains are relatively unaltered basalts, while the rocks of the Columbia Hills are generally accepted to have a more complex geological history [*Squyres et al.*, 2006a]. For the latter, our clusters also reproduce previously defined classes, and our analysis can be used to highlight the geochemical features which distinguish each cluster/class. Clovis class rocks (cluster G) were encountered at West Spur. They show enrichments in sulfur, chlorine and bromine, and have been previously described to contain weak olivine content [*Morris et al.*, 2006a]. They have been interpreted to be impact ejecta or tephra having undergone some aqueous alteration [*Squyres et al.*, 2006a]. Wishstone class rocks (cluster B) are enriched in phosphorus and titanium and have been suggested to be relatively unaltered pyroclastic deposits. They could have been formed by fractionation of primitive oxidized basaltic magma similar to the rocks of Adirondack class [*McSween et al.*, 2006b]. Peace class (C) is the class of rocks with the highest sulfur content encountered so far at Gusev and appears to consist of two main components: an ultramafic sandstone cemented by sulfate-rich materials [*Squyres et al.*, 2006a]. Watchtower class rocks (A) could be impact ejecta genetically related to the Wishstone class (B) and aqueously altered. They appear to be an intermediate mixture between Wishstone class rocks and another chemical component, not yet represented by any lithology encountered by the MER rover [*Hurowitz et al.*, 2006]. It should be recalled that in this analysis we have only considered rocks for which a RATed sample is available. This has the consequence that other rock classes previously defined in the literature, for instance, Backstay class [*Squyres et al.*, 2006a] is not considered here but will be mentioned later, when analyses of brushed and undisturbed rock samples are considered.

[20] One of the Meridiani clusters consists of the lone rock sample Bounce Rock (D) while the other consists of all the other RATed rocks (F), which appear to be relatively homogeneous in composition. As shown in Figure 1, chemical variability among Meridiani samples is overshadowed by that observed at Gusev. Nevertheless chemical trends exist for Meridiani samples, and these will be highlighted by analyzing APXS data from Opportunity separately (see section 3.3). Bounce Rock (D) is a basaltic rock close both in chemistry and mineralogy to the Shergottite EET79001 (Figure 1). It was encountered by Opportunity in the sedimentary context of Meridiani Planum

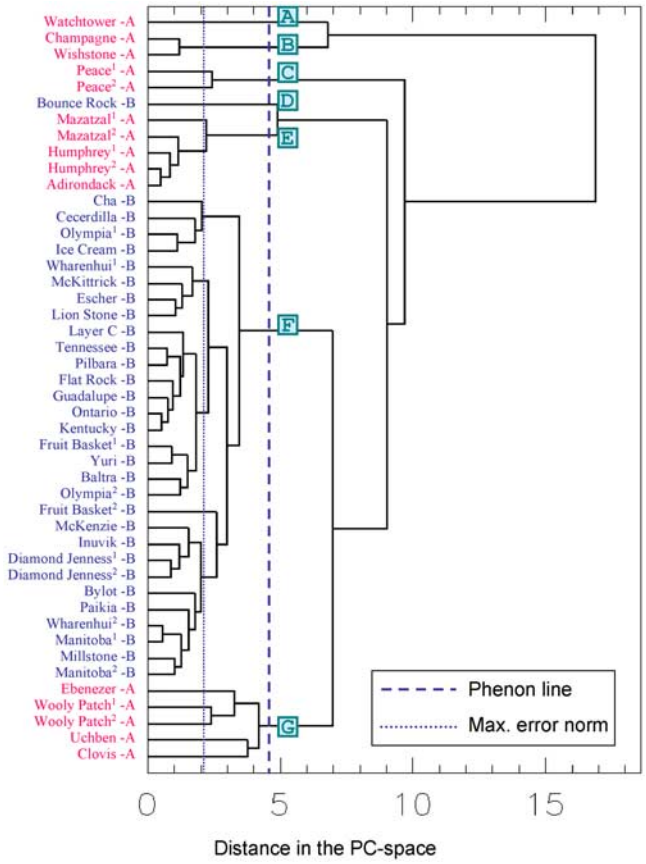

Figure 2. Dendrogram obtained for the hierarchical clustering performed on the subset of RATed rocks subsequently to the PCA performed on the whole set of samples from both sites with standardized elemental weight abundances. Leaves of the tree are labeled with the site (A for Gusev, B for Meridiani) and the name of the rocks. Clusters are identified with the same label as on Figure 1. See text for details about maximum error norm and phenon line.

but is not locally derived [*Squyres et al.*, 2006b]. Indeed, it appears to be singular in our analysis and its closest neighbor among the other clusters is cluster E (Figure 1), that containing the basaltic rocks from the Gusev plains (Adirondack class). Along with Adirondack, Peace and Wishstone classes, the Meridiani sedimentary rocks appear to be an end-member among the combined database of RATed samples from both sites.

3.2. Gusev Crater

[21] It has just been demonstrated that the PCA analysis allows unambiguous definition of clusters among RATed rocks. It is tempting, therefore, to extend this analysis to brushed and undisturbed rock samples, especially in light of the fact that only few rocks among all those encountered by Spirit in the Columbia Hills were RATed (the category of samples ''RAT fines'' is not mentioned here as only one measurement of this type is available). However, care must be taken, as PCA and hierarchical clustering using all rock samples regardless of their RATed, brushed or undisturbed nature may lead to erroneous conclusions. This is because of the homogenizing effect of a dust layer (and to a lesser extent of rinds) on rock compositions, as already mentioned in section 3.1. A RATed sample of a rock X could, for instance, appear compositionally dissimilar to the undisturbed sample of the same rock X but similar to an undisturbed sample of another rock Y. Such cases would lead to the definition of incoherent or meaningless clusters.

[22] In order to extend the analysis while considering these limitations, we performed three separate analyses (i.e., a PCA followed by a hierarchical clustering) for three subsets of Gusev samples, each corresponding to a different type of rock (RR, RB, and RU in Table 1). On the one hand, this user intervention could be considered as a limit to our ''independent'' classification method, but it appeared to be the best way to deal with the fact that we have three distinct types of rock surfaces in our data set. As in the previous analysis, the 16 chemical elements are used with their standardized abundances. The resulting dendrograms (one for each analysis) are shown in Figures 3a–3c, and the clustering results are compared in Figure 4. When several measurements of the same type are available for the same rock, they are numbered with a superscript. For reasons of clarity, the analyses concerning RATed, brushed and undisturbed rocks will be named RR, RB and RU respectively. In addition to the nomenclature already used in section 3.1 (terms cluster and class), the expression ''Clustering-Derived classes'' (CD classes) will be used when referring to the classes of rocks determined in the present study on the basis of the RR, RB, and RU analyses. Because of the potential effects of dust or rinds on rock compositions that can occur in the RB and RU analyses, the RR analysis will be used as the reference frame for our classification of other samples. Then brushed rocks will be considered, followed by undisturbed rocks.

[23] Unsurprisingly, the analysis performed exclusively on Gusev RATed rocks yields the same five clusters (A, B, C, D, and E on Figures 3a and 4) as the global analysis which also included Meridiani samples (Figure 2). There is a perfect correspondence between the clusters determined in the RR analysis and the classes of rocks from *Squyres et al.* [2006a]: all the rocks whose samples belong to a cluster also belong to the class corresponding to this cluster.

[24] Figure 3b shows that the RB analysis is coherent with that of the RR. Because of the presence of brushed rocks for which a RATed sample was also available, it is easy to identify the five CD classes mentioned above: Adirondack (cluster G on Figures 3b and 4), Peace (S), Wishstone (M), Watchtower (N) and Clovis, the latter being divided into two clusters (D and E). According to the dendrogram, clusters M and N appear to form a ''supercluster'' which supports a petrogenetic link between Wishstone and Watchtower classes. Note that the only brushed Mazatzal measurement is one of several samples defining lone sample clusters (J), while the Mazatzal RATed measurement belonged to the Adirondack cluster of plain basalts according to the RR analysis. This may be due to the presence of a compositionally distinct alteration rind on this rock as can be seen on color images of Mazatzal's surface [*Squyres et al.*, 2004, Figure 13]. In addition, other clusters are observed, containing rocks for which no RATed sample was available. With the exception of the Backstay CD class (L) that was available at the time of the previous studies of the

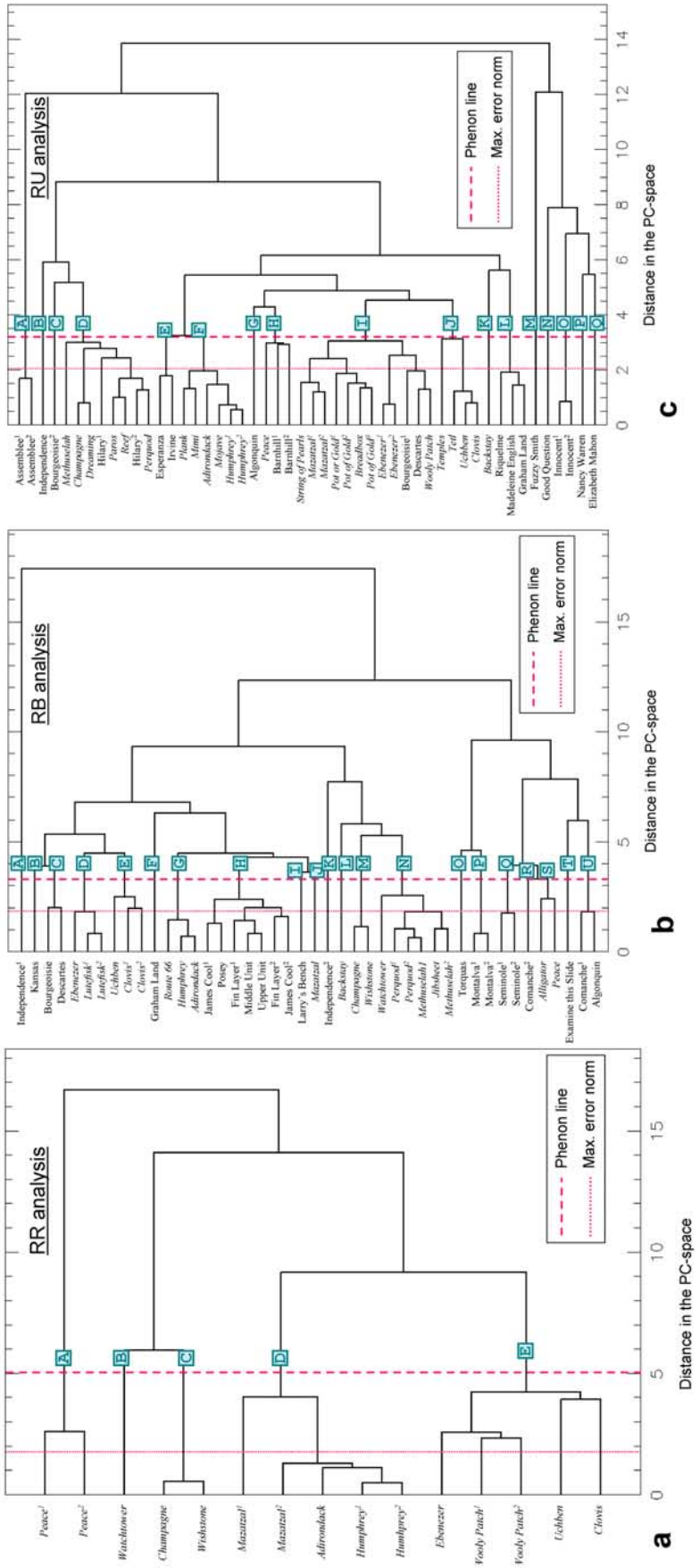

Figure 3. Dendrograms obtained for a PCA and a hierarchical clustering both performed on three different subsets of Gusev samples with standardized elemental weight abundances. Leaves of the tree are labeled with the name of the rocks. The names of rocks encountered until Backstay are written in italic. See text for details about maximum error norm and phenon line. (a) RATed rocks, (b) brushed rocks, and (c) undisturbed rocks.

Columbia Hills (its brushed sample was analyzed on sol 511) [*Squyres et al.*, 2006a; *Arvidson et al.*, 2006a; *Ming et al.*, 2006], these clusters correspond to new CD classes of rocks among the recent data. Backstay had been already identified as a relatively unaltered basalt/trachybasalt [*Squyres et al.*, 2006a] that could have formed during fractional crystallization of Adirondack class magmas, as Wishstone class rock [*McSween et al.*, 2006b]. It is of note that few of the additional clusters contain more than one sample: Bourgeoisie/Descartes (C), Seminole (Q), Algonquin/Comanche (U), Home Plate (H) and Montalva (P). Bourgeoisie and Descartes both have a relatively high potassium content compared to most of the other rocks, although the origin of this feature is not yet clearly determined. Seminole could be an intermediate sample in a mafic-ultramafic magmatic sequence going from Larry's Bench to Algonquin and Comanche [*Mittlefehldt et al.*, 2006]. Indeed, the Seminole and the Algonquin/Comanche clusters appear relatively close in chemical composition (Q and U on Figure 3b). Both are geochemically similar to Peace CD class rocks (S) and one of the two Comanche samples is even in the Peace CD class cluster. This leads us to think that Seminole or Algonquin/Comanche could represent the ultramafic component which is mixed with sulfate-rich materials in Peace CD class rocks. This is consistent with the structural interpretation of *McCoy et al.* [2007], suggesting that the rocks of Peace, Algonquin and Seminole CD classes all belong to the same stratigraphic unit.

[25] Home Plate is a subcircular plateau, ~90 m large and ~3 m high, located within the Inner Basin of the Columbia Hills. It is made of layered bedrock probably resulting from volcanic interactions with water or ice [*Squyres et al.*, 2007; *Crumpler et al.*, 2007]. The three brushed samples analyzed at Home Plate before sol 1260 belong to the same cluster (H). Both brushed samples analyzed on the rock Montalva form another cluster (P). Montalva was encountered near Home Plate and has the highest K content measured yet (until sol 1260). It seems to be an ultramafic rock like Torquas, whose brushed measurement defines a lone sample cluster (O). Torquas is located only a few meters away from Montalva and is similar in chemical composition, but possibly slightly more altered.

[26] Figure 3c shows that the RU analysis is also consistent with the RB and RR analyses although some minor differences appear because of the effect of the dust layer. Adirondack class rocks still form a distinct cluster (cluster F on Figures 3c and 4). Rocks from Watchtower and Wishstone classes belong to the same cluster (D). This is probably due, in part, to the homogenizing effect of the dust on the composition but it also reinforces the hypothesis of a petrogenetic link between those two classes. The two undisturbed measurements available for Mazatzal do not belong to the same cluster as other Adirondack class samples (cluster F), which is not surprising in light of the rind effect described above for the RB analysis. They appear instead in one of the two Clovis clusters (I). Indeed, as in the RB analysis (Figure 3b), Clovis class rocks are divided into two clusters (I and J on Figures 3c and 4), one of them contains the undisturbed samples of Bourgeoisie and Descartes (I). Although Bourgeoisie and Descartes fall in the Clovis cluster in this RU analysis, the fact that they are classified in the same cluster in both the RB and the RU analyses is in agreement with the definition of another CD class: Descartes CD class. On the other hand, it is debatable if Pot of Gold is a subclass of Clovis CD class or not, as stated by *Squyres et al.* [2006a]. This is visible on the dendrogram of Figure 3c, as moving the phenon line slightly could lead to the definition of two subclusters within cluster I, one containing similar rocks like Pot of Gold, Breadbox and String of Pearls (along with the two undisturbed measurements of Mazatzal). These rocks also share some common characteristics such as a high hematite content [*Morris et al.*, 2006a] and a very irregular morphology [*Squyres et al.*, 2006a]. In the RU analysis, the Peace and Home Plate samples belong to the same cluster (H), with the exception of Fuzzy Smith, a small rock encountered around Home Plate, defining a lone sample cluster (M). Fuzzy Smith is a ~10 cm irregularly shaped rock chemically very different from any other sample, notably with one of the highest Si contents measured at Gusev [*Squyres et al.*, 2007], and which may also contain Fe-sulfide [*Morris et al.*, 2007]. Both measurements performed on the rock Assemblee also define a cluster (A), certainly because of the high chromium content. Graham Land/Riquelme/Madeleine, Irvine/Esperanza and Innocent are the other clusters containing more than one sample (L, E and O, respectively). Irvine CD class rocks, Irvine and Esperanza, are vesicular basalts [*Crumpler et al.*, 2007]. Irvine was encountered close to the top of the Columbia Hills (Figure 5) while Esperanza was found on Low Ridge. As the rocks of Wishstone and Backstay classes, Irvine may have formed by fractionation of Adirondack class magmas [*McSween et al.*, 2006b]. The rocks of the Graham Land cluster (L) were encountered close to Home Plate and are probably ultramafic.

[27] The most significant CD classes of rocks are indicated in the last column of Figure 4, based on the results of the clustering for all three analyses. Figure 5 shows the location of the samples on the Gusev map with a color/symbol code indicating to which CD class they belong. Some samples that define lone sample clusters in the RU and the RB analyses have not been mentioned here; there is no striking evidence that they belong to any of the previous CD classes, but at the present time it is not clear whether it is justified or not to define new CD classes of rocks especially for them (Figure 4). While the Adirondack class contains all the rocks of the basaltic plains, most of the CD classes of rocks encountered in the Columbia Hills are confined to relatively restricted geographical areas. This remark is also valid for Clovis class, the class of rocks containing the highest number of samples. Only two of the CD classes of rocks determined contain samples separated by more than 100 m (Watchtower and Irvine CD classes on Figure 5), although it should be borne in mind that to some extent this observation may be related to the way in which the rovers perform their sampling (generally along linear traverses). Watchtower CD class rocks are found at two distinct locations: the samples on Cumberland Ridge, already identified as Watchtower class rocks by *Squyres et al.* [2006a], and two undisturbed measurements of the rock Hillary, encountered later in the traverse, close to the summit of Husband Hill. This occurrence of Watchtower CD class rocks at two distinct locations is consistent with

RR analysis		RB analysis		RU analysis		CD-classes
Cluster	Samples	Cluster	Samples	Cluster	Samples	
D	*Adirondack* *Humphrey*[1,2] *Mazatzal*[1,2]	G	*Adirondack* *Humphrey* *Route 66*	F	*Adirondack* *Mimi* *Humphrey*[1,2] *Plank* *Mojave*	**Adirondack**
		J	*Mazatzal*			
E	*Clovis* *Uchben*	E	*Clovis*[1,2] *Uchben*	J	*Clovis* *Uchben* *Tetl* *Temple*	**Clovis**
	Ebenezer *Wooly Patch*[1,2]	D	*Ebenezer* *Lutefisk*[1,2]	I	*Mazatzal*[1,2] *Ebenezer*[1,2] *Wooly Patch*[1,2] *Pot of Gold*[1,2,3] *Breadbox* *String of Pearls*	
					Descartes Bourgeoisie[1]	
		C	Descartes Bourgeoisie	C	Bourgeoisie[2]	**Bourgeoisie**
		H	James Cool[1,2] Posey Fin Layer[1,2] Middle Unit Upper Unit	H	Barnhill[1,2] *Peace*	**Home Plate**
A	*Peace*[1,2]	S	*Peace* *Alligator*			**Peace**
		Q	Seminole[1,2]			**Seminole**
		U	Algonquin Comanche[1]	G	Algonquin	**Algonquin**
		R	Comanche[2]			
B	*Watchtower*	N	*Watchtower* *Perquod*[1,2] *Jibsheet* *Methuselah*[1,2]	D	*Perquod* *Methuselah* *Paros* *Reef* Hillary[1,2]	**Watchtower**
C	*Wishstone* *Champagne*	M	*Wishstone* *Champagne*		*Champagne* *Dreaming*	**Wishstone**
		L	*Backstay*	K	*Backstay*	**Backstay**
		F	Graham Land	L	Graham Land Riquelme Madeleine	**Graham Land**
		A	Independence[1]	B	Independence	**Independence**
		K	Independence[2]			
		P	Montalva[1,2]			**Montalva**
				E	Irvine Esperanza	**Irvine**
				A	Assemblee[1,2]	**Assemblee**
				O	Innocent[1,2]	**Innocent**
				M	Fuzzy Smith	**Fuzzy Smith**
		B	Kansas			?
		I	Larry's Bench			?
		O	Torquas			?
		T	Examine this Slide			?
				N	Good Question	?
				P	Nancy Warren	?
				Q	Elizabeth Mahon	?

Figure 4. Determination of Gusev rock CD classes by comparing the results of the abraded (RR), brushed (RB), and undisturbed (RU) rock surfaces analyses. The names of rocks encountered until Backstay are written in italic.

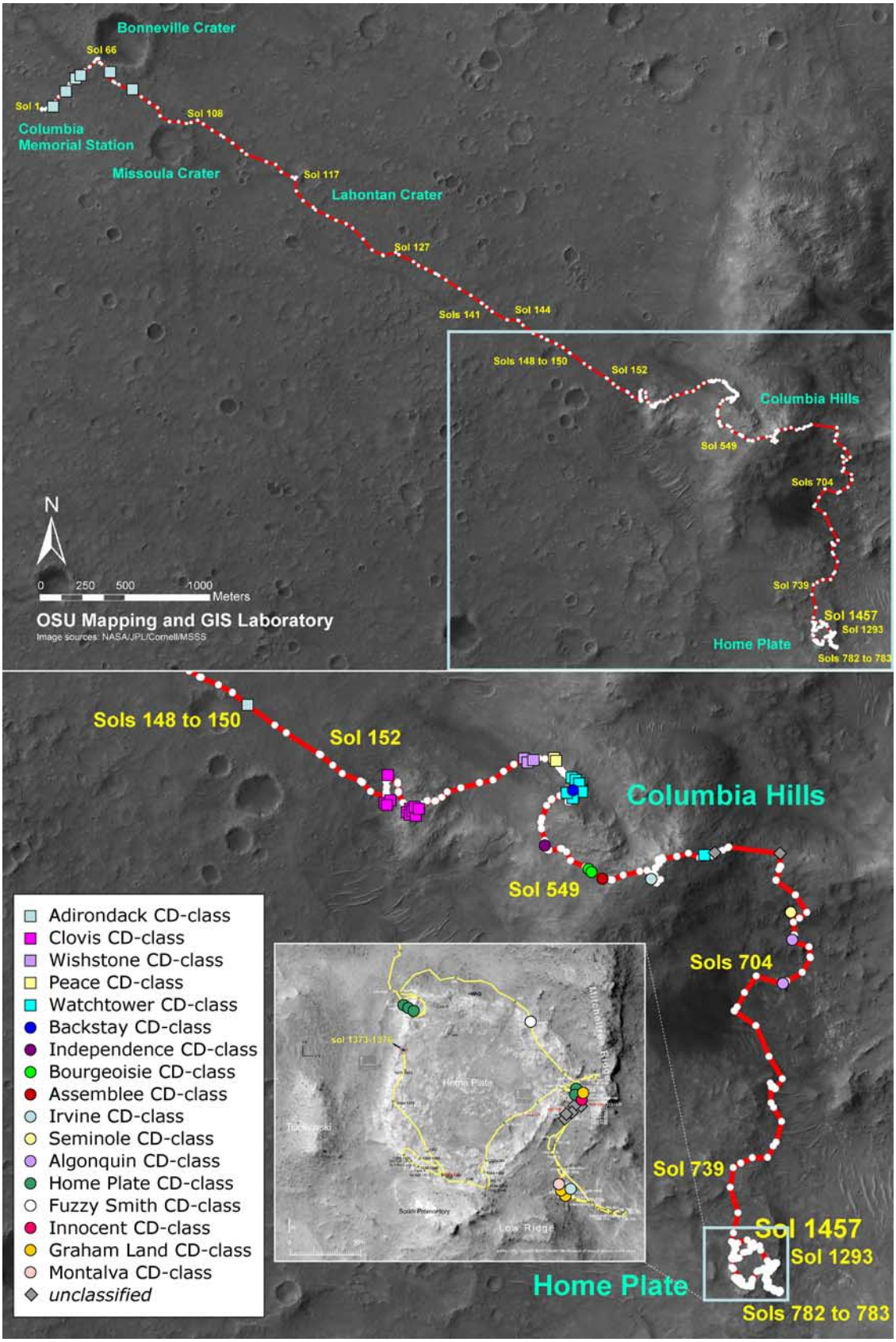

Figure 5. Map of Gusev with the localization of the rock samples encountered by Spirit. The symbol/color code indicates to which CD class the samples belong.

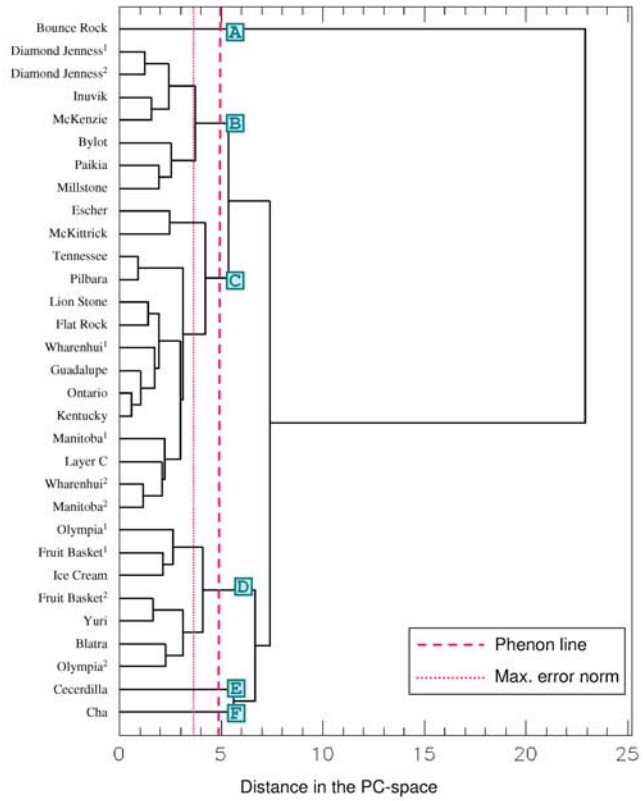

Figure 6. Dendrogram obtained for a PCA and a hierarchical clustering both performed on the subset of Meridiani RATed rocks with standardized elemental weight abundances. Leaves of the tree are labeled with the name of the rocks. See text for details about maximum error norm and phenon line.

the stratigraphy proposed by *McCoy et al.* [2007] that places them within the same unit based on the strikes and dips derived from imagery.

3.3. Meridiani Planum

[28] Meridiani data have been studied using two independent analyses: the first uses standardized data and will show the coherence between the compositional variations among RATed rocks and their geographical distribution. The second was performed using nonstandardized data (see section 2.2), an analysis that highlights the role of major elements, and which provides insight into the petrogenetic interpretation of compositional variations.

[29] A PCA has been performed exclusively on Meridiani RATed rocks considering standardized abundances of all 16 chemical elements, followed by hierarchical clustering. This analysis leads to the definition of six clusters (Figure 6) that show an excellent correlation with the spatial distribution of the samples (Figure 7). As in the global analysis (Figure 2) Bounce Rock defines a lone sample cluster (A) because of its basaltic nature. The samples encountered before reaching the Heat Shield belong to two groups: cluster B contains the samples measured in the deepest layers of outcrops in Endurance Crater as well as displaced rocks at the bottom of this crater, and cluster C contains the samples measured in the upper layers of Endurance Crater, in Eagle Crater and between these two craters. This distribution is in excellent agreement with the scenarios proposed for explaining the observed stratigraphy, as the elevation limit between clusters B and C is the Whatanga contact that separates the middle and upper Burns units [*McLennan et al.*, 2005; *Grotzinger et al.*, 2005]. The two RATed sample measurements available so far in the surroundings of Victoria Crater, Cha and Baltra, both define lone sample clusters (E and F on Figure 6). All the remaining RATed samples, measured during the drive from Endurance to Victoria, plot in cluster D. This good agreement between compositional variations and locality shows that, despite the relatively weak chemical variability among Meridiani sedimentary rocks, chemistry and possibly geological context vary systematically along Opportunity's traverse.

[30] A second PCA has been performed on all the APXS samples (rock and soil measurements, excepted HSR) at Meridiani, considering all 16 chemical elements with their real (nonstandardized) weight abundances, extending the work of *Tréguier et al.* [2007]. Table 4 shows how much of the variance is accounted for by each principal component. In this analysis, dominated by the major elements Fe, S, Si, Ca, and Al, the first two principal components account for ~92% of the total variance. Note that the percentages of variance of this PCA (Table 4) cannot be compared with those of the PCA performed on the whole data set (Table 3) where the abundances were standardized. Also, the fact that the PC are dominated by only five major elements does not mean that there is no chemical variability among minor elements, as this is a different kind of analysis that emphasizes variations of the most abundant elements. In the PC1 versus PC2 plane the data form two branches which converge in a sort of V shape (Figure 8). The left-hand branch is formed by soils and is parallel to the vector of Fe, while the right-hand branch is formed by rocks and is approximately parallel to the vector for S (the projections of the chemical vectors in the plane of the first two principal axes are overlain on Figure 8). Adirondack (RATed) composition has also been plotted in this plane, but was not used for the definition of the components. Undisturbed rocks occur in the vicinity of the convergence point of the two branches (close to Adirondack) with the exception of Berry Bowl, a sample concentrated in hematite-rich spherules [*Morris et al.*, 2006a]. RATed rocks form the other extremity of the branch, with the exception of Bounce Rock that is close to Adirondack, as may be expected. Brushed rocks plot between undisturbed and RATed rocks. This PCA highlights enrichment in iron for the samples belonging to the soil branch. As shown by the projection of the chemical vectors in the PC1 versus PC2 plane (Figure 8), iron does not appear to be associated with any other major element. It implies that these soil samples are enriched in iron alone or in iron associated with an unmeasured element (possibly oxygen). Thus, the iron enrichment is not due to some iron-rich mafic mineral. On the contrary, the variations along the soil branch may be directly related to the proportion of ubiquitous hematite-rich spherules (or their fragments) present in the samples [*Brückner et al.*, 2005]. Another characteristic of soils plotting on the left-hand branch is their enrichment in the trace element nickel [*Tréguier et al.*, 2007]. As nickel is a mobile element that can concentrate in

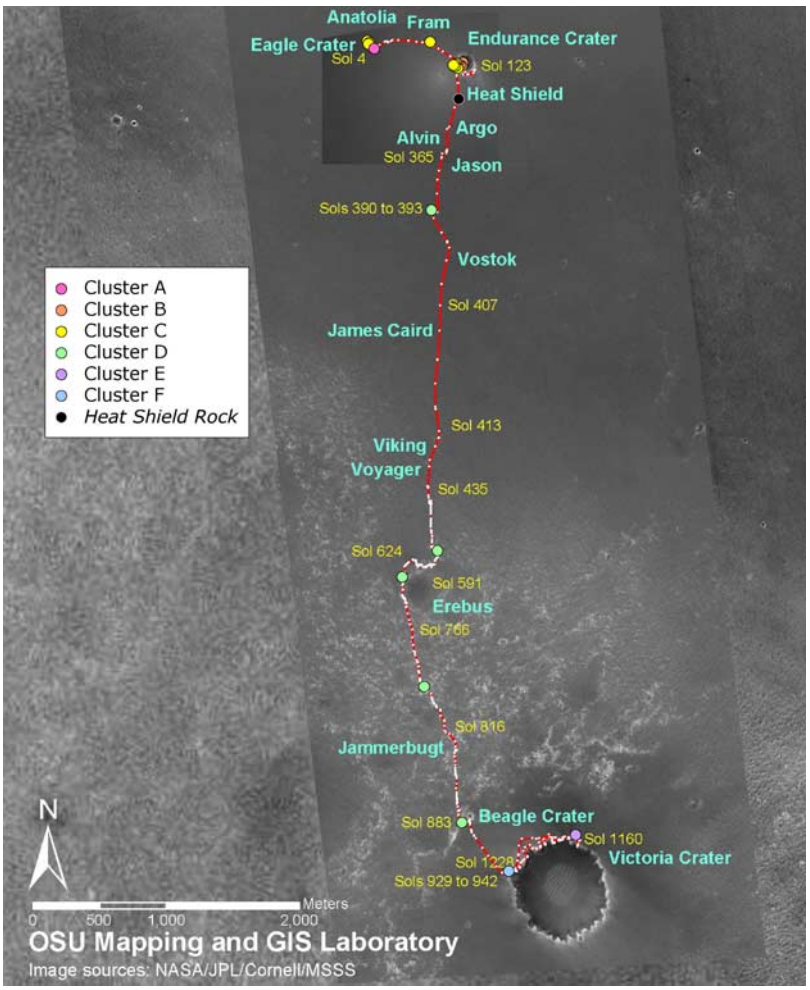

Figure 7. Map of Meridiani with the localization of the RATed rock samples encountered by Opportunity. The color code indicates to which cluster the samples belong.

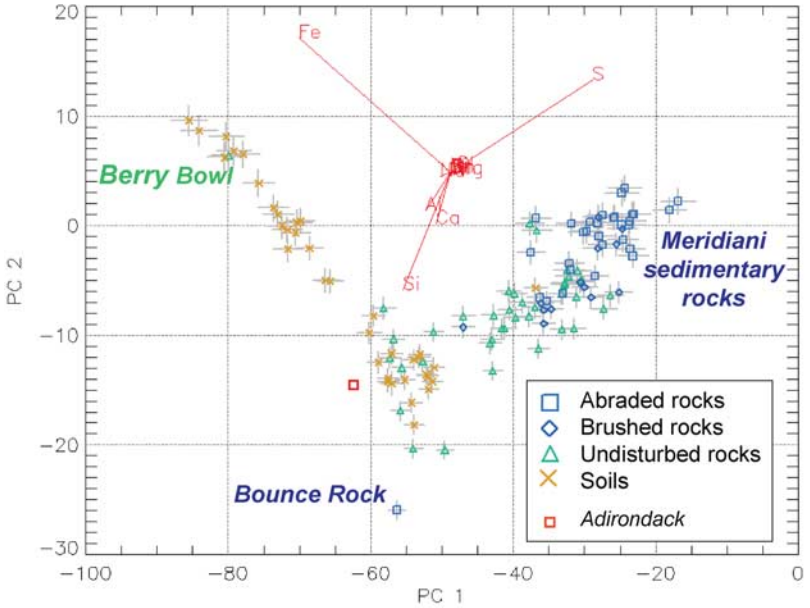

Figure 8. Scatterplot of the measurement points in the plane of the first two principal axes of the PC space for a PCA performed on the whole Meridiani set of samples with nonstandardized elemental weight abundances. Projections of the chemical vectors in this plane have been overplotted.

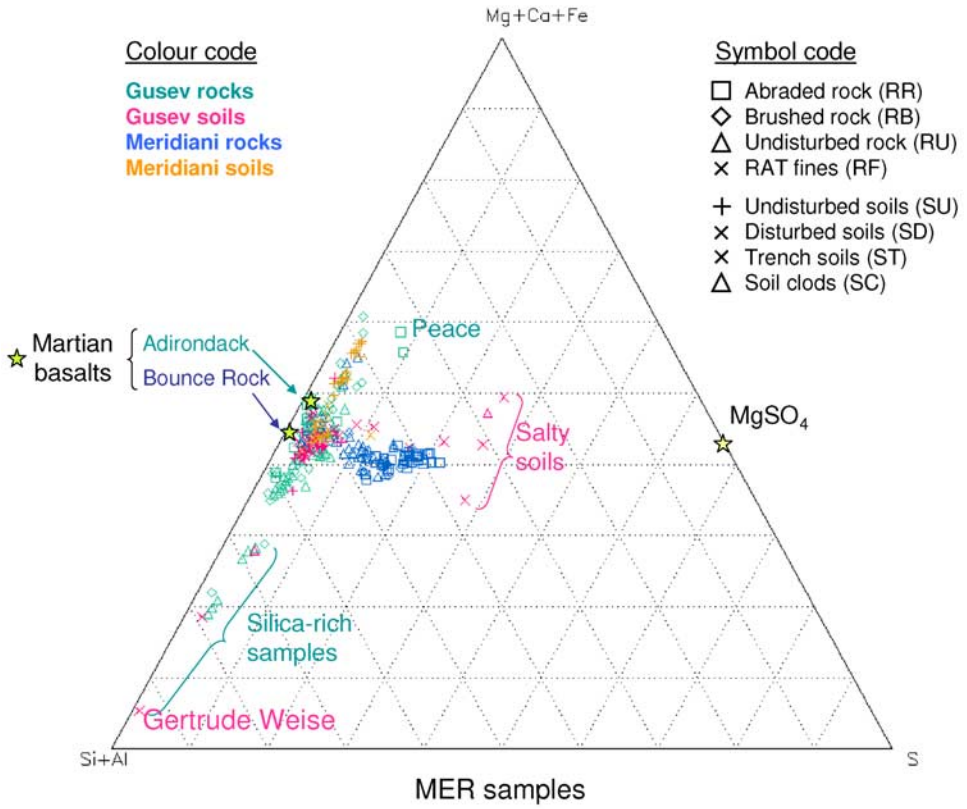

Figure 9. Ternary diagram {Mg + Ca + Fe, Si + Al, S} for elemental weight abundances with all Gusev and Meridiani samples. Basaltic compositions measured at Gusev (Adirondack class rocks) and at Meridiani (Bounce Rock) are highlighted by two green stars, and magnesium sulfate composition is highlighted by a yellow star.

hematite-rich spherules through aqueous processes [*Yen et al.*, 2006], this observation is also in agreement with the hematite hypothesis for the soil branch. On the other hand, the right-hand branch containing the RATed rock samples is parallel to the S vector consistent with external addition of sulfur. Petrologic mechanisms capable of producing the observed compositional trend will be explored in section 4.

4. Geochemical Modeling of Rock-Gas Interaction in Presence of Water

4.1. Context

[31] As shown in section 3.3, besides being a simple classification tool, PCA can also be used to identify mixing or exchange between components. This is particularly clear for the case of Meridiani rocks where it has been shown that their compositional variation is characterized by a simple enrichment in sulfur, relative to typical basalt compositions. As confirmation of the PCA results we plot the chemical compositions of all rocks and soils measured at both sites, except HSR, (in weight % of the elements) in the ternary diagram {Mg + Fe + Ca, Si + Al, S} (Figure 9). All the Meridiani rocks, with the exception of Bounce Rock, fall in a compact cluster. In this representation, their compositions broadly plot on a mixing line between the basalts from the Gusev plains and pure sulfur, confirming the result of the PCA. In detail, a slight trend can be observed among the Meridiani rocks toward a composition corresponding to a (Mg,Ca,Fe)-sulfate (Figure 9). This observation is consistent with the interpretation of *Brückner et al.* [2007] who suggested variable amounts of Mg-sulfate. Nevertheless, the correlation between sulfur and magnesium is only observed for the early data and corresponds to a joint depletion in sulfur and magnesium for the samples measured toward the bottom of Endurance Crater. This may suggest local migration of Mg-sulfates, postdating the formation of the bedrock [*Clark et al.*, 2005]. On the other hand, the first-order difference between the Meridiani rocks and likely basalt parents remains the addition of sulfur, with little or no addition or removal of associated cations. In this respect we note that the petrogenesis of Meridiani rocks has been the subject of debate in the recent literature. *McCollom and Hynek* [2005] have proposed hydrothermal alteration of volcanic materials to account for the Meridiani observations, while the MER team argues in favor of a brine/evaporate model [*Rieder et al.*, 2004; *McLennan et al.*, 2005; *Grotzinger et al.*, 2005; *Brückner et al.*, 2007]. In the next paragraph we will explore the possibility of a gaseous origin for this sulfur addition, through use of numerical geochemical modeling.

4.2. Description of the Model

[32] The assumptions of the model of basalt alteration under acid fog are summarized in Figure 10. The first step of this process is the addition of pure water, at a temperature of 0°C (step 1 on Figure 10). Melting of ice could be the

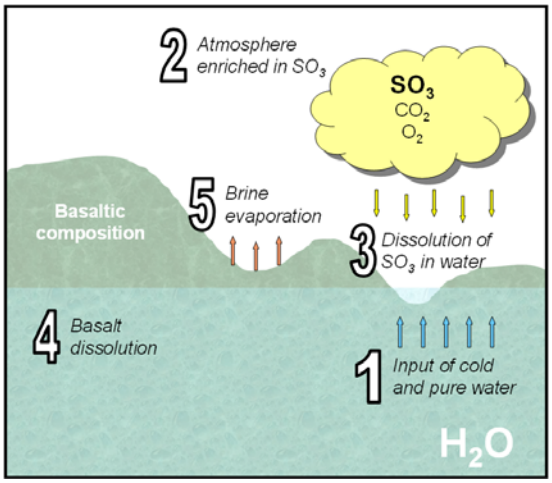

Figure 10. Illustration for the acid fog alteration model.

process responsible for this input. The second step is contact with an atmosphere enriched in SO_3 (step 2 on Figure 10). These conditions are not those encountered at the present-day Martian surface, in that we assume a relatively high temperature, the physical stability of water and the occurrence of sulfur gas. However, such conditions can be temporarily met during a volcanic event supplying heat, steam (6 mbars H_2O are required at 0°C to stabilize water, see *Haberle et al.* [2001] for more detailed discussions) and sulfur gas. Concerning the sulfur-bearing gas, analogy with terrestrial systems would suggest that the most probable form of sulfur gas released in the atmosphere by volcanic degassing is SO_2, not SO_3. However, on Earth, oxidation of SO_2 into SO_3 occurs and is promoted in the high atmosphere by the presence of O_2 and the action of UV radiations [*Cox*, 1979; *Lin and Chameides*, 1991; *Sievering et al.*, 2006] leading to the formation of fine sulfate aerosols. We assume that an analogous mechanism for SO_2 oxidation also occurred on Mars. Variable amounts of SO_3 have been considered in our models, expressed in terms of a gas to rock mass ratio. The other atmospheric conditions (CO_2 and O_2 partial pressures) have been chosen to mimic those of the current Martian surface: 0°C, 5.3 mbar CO_2, 7.8 μbar O_2 [*Zolotov and Mironenko*, 2007]. Under these conditions, the dissolution of SO_3 in water occurs (step 3 on Figure 10) leading to the production of sulfuric acid.

[33] We then consider the alteration of an Adirondack class rock (see section 3.1), under these acidic conditions (step 4 on Figure 10). The mineralogy of Adirondack given by *McSween et al.* [2006a] has been taken as the starting point. In the following we present the results of two distinct cases of alteration. The first involves alteration of all the minerals composing the basalt, while in the second, only olivine, pyroxenes and magnetite were considered to be altered. In this case of partial alteration, pyroxene and olivine were chosen as they are known to alter more rapidly than plagioclase at low pH, and magnetite was identified as it is known to dissolve before silicates under acidic conditions [*Zolotov and Mironenko*, 2007]. In each case, the brine resulting from SO_3 dissolution and basalt alteration is assumed to be immobile (step 5 on Figure 10). Evaporation of the brine is not explicitly modeled here. We simply assume that all nonaqueous components become part of the final rock. On the other hand, the composition of the brine defines not only the chemical composition of an evaporitic component of the final rock, but also the associated secondary mineralogy.

[34] The mineralogical transformation of Adirondack basalt under the conditions described above was modeled using the Chess geochemical software package (version 2.0, release 2) [*Van der Lee and de Windt*, 2002]. Briefly, Chess incrementally models mass transfer between gas, rock and aqueous phases. At each step, the program distributes each element of the solution between stable aqueous species, calculates the activity coefficients of water and the aqueous species, the gas fugacities, and the saturation index of the solution with respect to all of the phases of the database (derived from Supcrt92 [*Johnson et al.*, 1992]). Thermodynamic equilibrium is achieved by precipitating/dissolving the over/under saturated phases and calculating the new composition of the solution and gas. In the present calculations we assume that equilibrium secondary phases precipitate immediately (no kinetic constraints). On the other hand, given the low temperature and short-term reaction considered, chalcedony instead of quartz is assumed to limit the concentration of aqueous silica [*Garrels and Christ*, 1965] and goethite rather than hematite that of ferric iron [*Cornell and Schwertmann*, 2003]. For the same reasons, ultramafic minerals were removed from the list of potential secondary phases.

[35] In contrast to other published models, the reaction pathway considered here places particular importance on the role of gas-rock interaction, the water phase (initially pure water) simply acting as a medium allowing the chemical reactions to proceed. It is of note that the water/rock ratio (W/R) used for the results presented here was fixed arbitrarily to a value of 6. We have, however, tested higher (up to 12) and lower (down to 0.62) W/R values, but no significant changes in terms of secondary mineralogy are observed. This can be easily understood in light of the absence of ions and protons in the starting fluid. As such, the W/R was not considered as a key parameter, in contrast to the SO_3/basalt ratio. Moderate variations of either the temperature or partial pressures for O_2 and CO_2 are not found to affect the results of the simulations. For O_2, 7.8 μbar is high enough to stabilize rock components in their oxidized form, oxides, sulfates or carbonates (if carbon is present). It is for this reason that moderate changes in O_2 do not influence the chemical conditions of alteration. For CO_2, the sensitivity of the model depends on pH. Under acidic conditions imposed by SO_3 (sulfuric acid in its aqueous form), CO_2 dissolved in solution does not convert into HCO_3^- or CO_3^{2-} anions and consequently does not affect the mineral equilibria. A contrasting situation would occur under neutral or alkaline conditions, with carbonate stability increasing with increasing P_{CO2} but such conditions are not the subject of the present study. The amount of added SO_3 spanned a SO_3/basalt mass ratio of 0.024 to 0.96, covering the range of sulfur weight abundance measured by the APXS instruments on board the two MER rovers.

4.3. Results of the Model

[36] The secondary mineralogies obtained in the simulations are summarized on Figures 11a (total alteration) and

11b (partial alteration). For each case six values of SO_3/basalt mass ratio have been modeled, in the range from 0.024 to 0.96, as indicated on the horizontal axis of Figures 11a and 11b. The initial mass of Adirondack class basalt is 100 g and the quantities of secondary minerals are also expressed in grams (as are those of the remaining primary minerals whose alteration has been inhibited in the case of Figure 11b). For the lowest SO_3/basalt ratios, the total final mass exceeds 100 g because of the presence of water molecules in some of the secondary minerals. On the other hand, for the highest SO_3/basalt ratios, the total final mass of modeled solids is less than 100 g. This is due to the concentrated nature of the brine under these conditions, many ions produced by alteration of the primary minerals being present in solution. In the cases of both total and partial alteration, carbonates are only predicted for the lowest SO_3 input values (up to a ratio of 0.24). They disappear when the SO_3 input increases and the conditions become more acidic. Clay minerals only precipitate in the case of total rock alteration (Figure 11a). In this case, the mass of clay minerals tends to decrease with higher SO_3/basalt mass ratios but they are still present up to a ratio of 0.77. In the case of total rock alteration, chalcedony only precipitates for high values of SO_3/basalt mass ratio (greater than 0.48) and increases with SO_3 input. In the case of partial rock alteration, about the same mass of chalcedony precipitates for all SO_3 inputs tested. Gypsum precipitates for ratios greater than 0.24 in both cases of alteration. The precipitation of goethite and jarosite is observed for the highest SO_3/basalt mass ratio tested (0.96) in the case of total rock alteration (Figure 11a). On the other hand, the precipitation of goethite occurs for all tested ratios up to 0.48 in the case of partial rock alteration (Figure 11b) whereas jarosite does not precipitate for any of the tested ratios.

[37] For both cases of alteration and for each SO_3/basalt mass ratio, the composition of the final mineralogy and the composition of the remaining brine have been plotted in the ternary diagram {Mg + Fe + Ca, Si + Al, S} (Figures 12a and 12b) used in section 4.1 (Figure 9). In a natural situation, the amount of evaporitic component in the final rock may vary on a local scale if the brine has been mobile. Taking into account this general case involving brine circulation, it remains that the final rock compositions will lie along a mixing line between the modeled secondary mineralogy (with remaining primary minerals in the case of partial alteration) and the brine composition (Figures 12a and 12b). In the simplest scenario the mixing line will correspond to brine and secondary minerals produced during the same alteration process (i.e., a brine corresponding to the relevant SO_3/basalt mass ratio). On the other hand, more complex scenarios can be envisaged such as the addition of an evaporitic component (brine) resulting from a sulfur input higher or lower than that which generated the secondary minerals.

5. Discussion

5.1. Gusev Rocks and Soils

[38] By comparing Figures 9 and 12b, it appears that the compositions obtained with the model in the case of partial rock alteration for SO_3/basalt mass ratios of 0.77 and 0.96 match the composition of silica-rich Gusev samples relatively well. Among the nine Gusev samples concerned, two are soil samples and seven are rock samples. The rock samples are from Independence, Assemblee and Fuzzy Smith CD classes (all the samples of those CD classes plot in this area of the ternary diagram, which supports the classification performed in section 2) along with two other samples, Nancy Warren and Elizabeth Mahon, that both defined lone sample clusters in the RU analysis (Figure 4). The acid fog alteration model assuming partial alteration thus appears relatively well adapted for explaining these compositions. It is of note that in light of the fact that these rock samples are either undisturbed or only brushed, it cannot be ruled out that the proposed alteration process only occurred superficially, creating an alteration rind.

[39] On the other hand, the compositions of several Gusev S-rich soils (see section 3.1) are consistent with the modeling of total rock alteration. Comparison of Figures 9 and 12a, shows that these Gusev soils lie between brines and corresponding secondary minerals, modeled for SO_3/basalt mass ratios between 0.24 and 0.77. Thus, the assumption of bulk rock alteration would appear to be more appropriate for the formation of these soil samples, in agreement with the processes suggested by *Wang et al.* [2007].

5.2. Meridiani Rocks

[40] Comparison of Figures 9 and 12a, shows that the compositions modeled for total rock alteration and a SO_3/basalt mass ratio of 0.24, may explain the chemical composition of Meridiani sedimentary rocks, if addition of an evaporitic component resulting from brine evaporation is considered. For this SO_3/basalt ratio, the secondary mineralogy is predicted to be dominated by clays. Gypsum may precipitate but the conditions are not acidic enough to avoid the precipitation of some carbonates (Figure 11a). According to Opportunity's observations, occurrence of fine clay is not ruled out [*Grotzinger et al.*, 2005] although a lack of carbonate at Meridiani is generally admitted. Thus, this case does not work in terms of mineralogy although the results are chemically satisfying. Comparison of Figures 9 and 12b shows that the compositions obtained for the case of partial rock alteration for a SO_3/basalt ratio of 0.24 may also explain the chemical composition of Meridiani sedimentary rocks (assuming addition of an evaporitic component). The precipitation of carbonates still occurs for a ratio of 0.24 but does not occur for a ratio of 0.48 as the brine becomes more acidic. Thus, sulfur input with a SO_3/basalt ratio between 0.24 and 0.48 (indexes 3 and 4 on Figure 12b) appears to match Meridiani observations. According to the results of the model, a few grams of goethite would precipitate although this mineral has not been detected by Opportunity's Mössbauer spectrometer [*Morris et al.*, 2006b]. However, the calculated presence of goethite may be a direct consequence of the fact that hematite precipitation was inhibited in the model for kinetic reasons (see section 4.2). While this choice is justified for short-term reactions, it is possible that a transformation of goethite into hematite might have occurred during a later process, maybe related to the formation of the berries. On the other hand, jarosite has been identified by Opportunity's Mössbauer spectrometer, whereas the results of the modeling presented here suggest that this mineral is only obtained for a SO_3/basalt ratio of

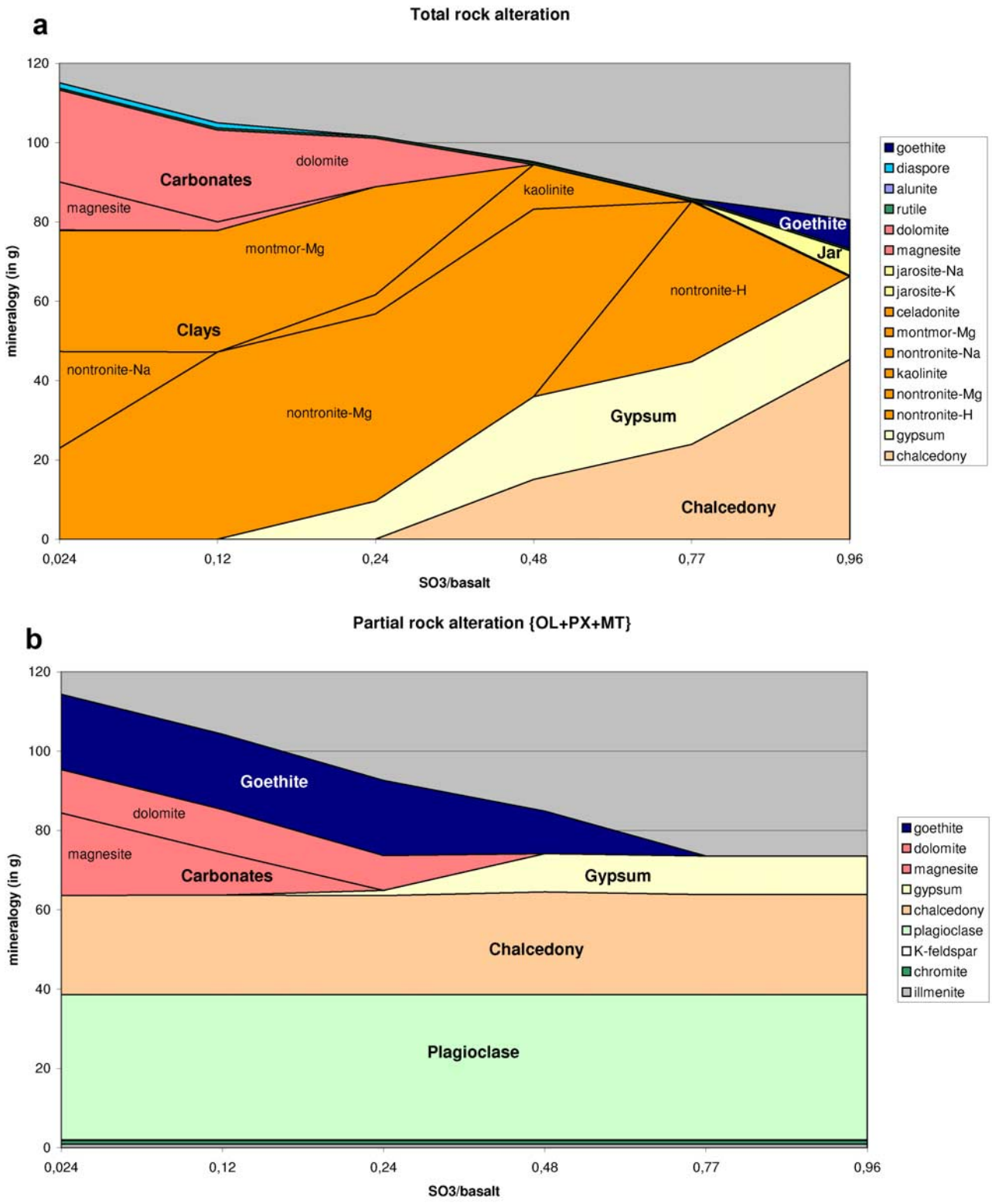

Figure 11. Mineralogy obtained through the acid fog alteration model, with an initial mineralogy similar to Adirondack class rocks. (a) Case of total rock alteration. (b) Case of partial alteration of olivine, pyroxenes, and magnetite.

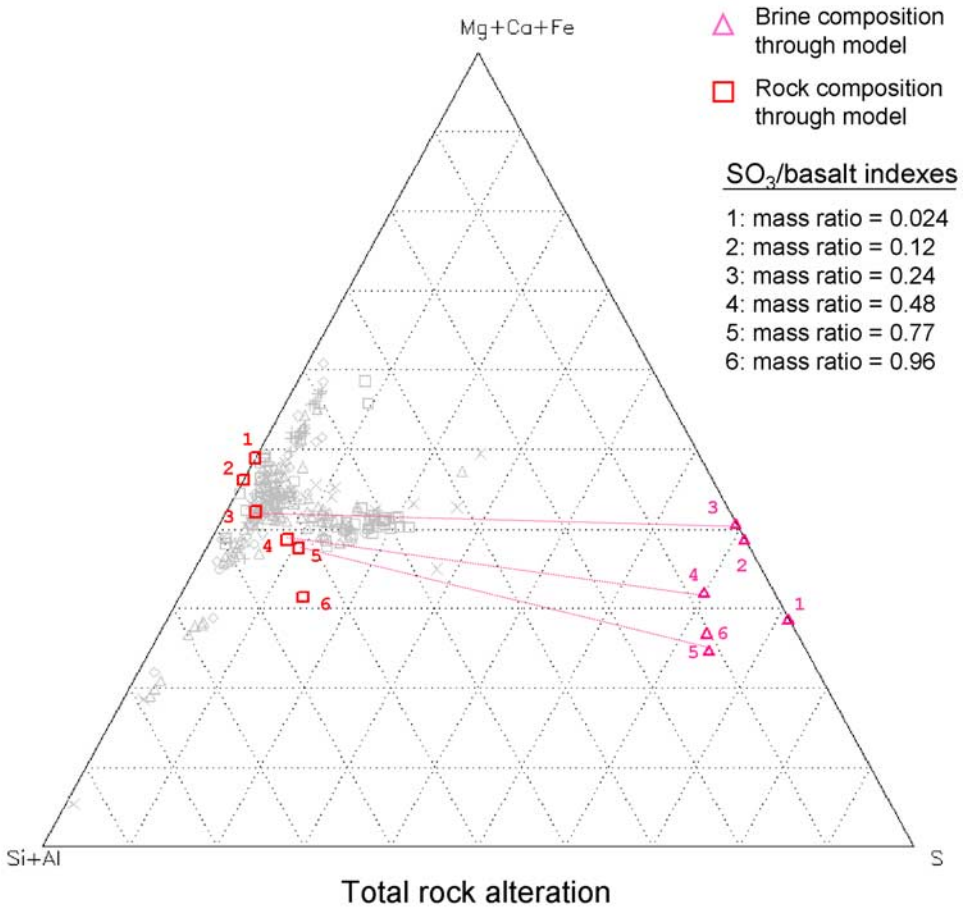

Figure 12. Ternary diagram {Mg + Ca + Fe, Si + Al, S} for elemental weight abundances with the results of the acid fog alteration model. For each SO_3/basalt mass ratio, the composition of both the final rock and the brine are plotted over the shadow of all Gusev and Meridiani samples from Figure 9. (a) Case of total rock alteration. (b) Case of partial alteration of olivine, pyroxenes, and magnetite.

0.96 and total alteration. However, the chemical composition of the secondary mineralogy provides a less satisfactory match to Meridiani APXS measurements in that case. Although the overall results are satisfying, they suggest that the simple models presented here may require some refinement in order to explain the details of the Meridiani compositions. For example, the partial alteration of other sets of minerals, other than olivine, pyroxenes and magnetite, should be investigated, along with other kinetic constraints. The influence of using other initial basaltic compositions could also be tested, as the unaltered bedrock at Meridiani may not necessarily be identical to that of Adirondack basalt observed at Gusev.

6. Conclusions

[41] The results presented in this paper demonstrate the adequacy of mathematical tools such as PCA to assess and interpret compositional variations provided by the APXS instrument. By taking into account most of the available chemical information simultaneously, PCA can be used as a unsupervised tool to identify and characterize the different families of rocks encountered by the rovers. Along with hierarchical clustering a robust classification of samples is possible that helps to identify distinct classes of rocks, and to shed light on the petrogenetic relationships between them. This analysis is found to be particularly useful in the case of samples from Gusev where a high diversity of rock types has been observed, particularly in the Columbia Hills. This confirms the utility of the RAT, as the chemical diversity of rocks measured by APXS is clearly best characterized through analysis of abraded surfaces. The results of the classification show good agreement with the classes identified in the previous studies of Columbia Hills and suggest the definition of new rock classes among the most recent samples. It will be interesting to complete the Meridiani analysis with the upcoming measurements on the rocks that Opportunity is hopefully going to analyze during its descent into Victoria Crater. The interpretation of the PCA results led us to explore a simple model of acid fog alteration of Martian basalts. For the cases of both total and partial alteration, the secondary mineralogy predicted by the model is broadly coherent with rock and soil compositions measured at both Gusev and Meridiani, especially if we considerer the role of brine circulation and evaporation. In order to explain in full the chemical and mineralogical diversity of the rocks characterized by the Athena payload,

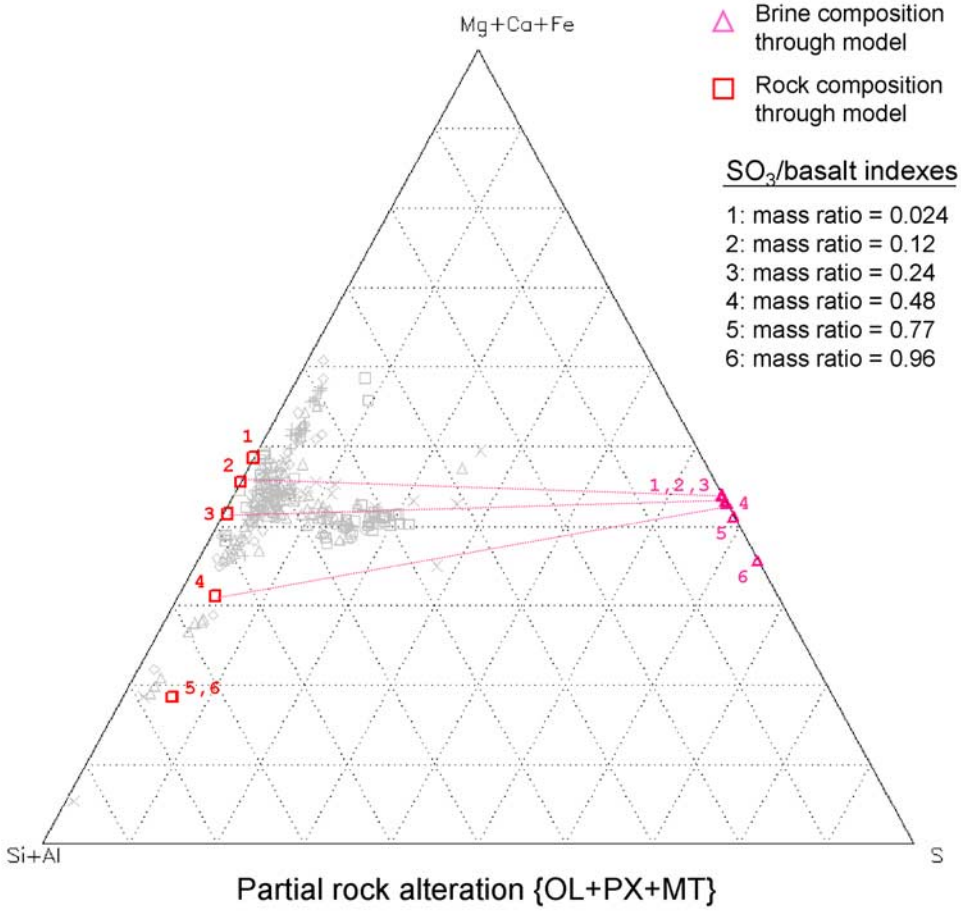

Figure 12. (continued)

more detailed modeling under more restricted conditions will be performed.

[42] **Acknowledgments.** We thank the scientists and engineers of the MER project who enable daily science observations at the Spirit and Opportunity landing sites. The APXS was funded by the Max Planck Society and by the German Space Agency (DLR). We also acknowledge the support of the Programme National de Planétologie and the French Space Agency (CNES). We gratefully thank Edward A. Guinness and an anonymous reviewer for their constructive comments that enabled significant improvements to this paper.

References

Arvidson, R. E., and S. W. Squyres (2005), Recent results from the Mars Exploration Rover Opportunity Mission, *Eos Trans. AGU*, *86*(18), Jt. Assem. Suppl., Abstract P31A–02.

Arvidson, R. E., et al. (2006a), Overview of the Spirit Mars Exploration Rover Mission to Gusev Crater: Landing site to Backstay Rock in the Columbia Hills, *J. Geophys. Res.*, *111*, E02S01, doi:10.1029/2005JE002499.

Arvidson, R. E., et al. (2006b), Nature and origin of the hematite-bearing plains of Terra Meridiani based on analyses of orbital and Mars Exploration Rover data sets, *J. Geophys. Res.*, *111*, E12S08, doi:10.1029/2006JE002728.

Brückner, J., et al. (2005), Hematite on the surface of Meridiani Planum and Gusev Crater, *Lunar Planet. Sci.*, *XXXVI*, [CD-ROM], Abstract 1767.

Brückner, J., et al. (2006), Two years of chemical sampling on Meridiani Planum by the Alpha Particle X-Ray Spectrometer onboard the Mars Exploration Rover Opportunity, *Lunar Planet. Sci.* [CD-ROM], *XXXVII*, Abstract 1882.

Brückner, J., G. Dreibus, R. Gellert, C. d'Uston, and the Athena Science Team (2007), Chemistry of Martian surfaces as determined by the APXS of the Mars Exploration Rovers, in *Seventh International Conference on Mars*, Abstract 3120, Jet Propul. Lab., Pasadena, Calif.

Chevrel, S. D., P. C. Pinet, Y. Daydou, S. Maurice, D. J. Lawrence, W. C. Feldman, and P. G. Lucey (2002), Integration of the Clementine UV-VIS spectral reflectance data and the Lunar Prospector gamma-ray spectrometer data: A global-scale multielement analysis of the lunar surface using iron, titanium, and thorium abundances, *J. Geophys. Res.*, *107*(E12), 5132, doi:10.1029/2000JE001419.

Clark, B. C., et al. (2005), Chemistry and mineralogy of outcrops at Meridiani Planum, *Earth Planet. Sci. Lett.*, *240*, 73–94, doi:10.1016/j.epsl.2005.09.040.

Cornell, R. M., and U. Schwertmann (2003), *The Iron Oxides: Structure, Properties, Reactions, Occurrence and Uses*, Weinheim, New York.

Cox, R. A. (1979), Photochemical oxidation of atmospheric sulphur dioxide, *Philos. Trans. R. Soc. London, Ser. B*, *290*, 543–550, doi:10.1098/rsta.1979.0013.

Crumpler, L. S., T. J. McCoy, M. Schmidt, and N. Cabrol (2007), Physical volcanology at Gusev Crater, Spirit Rover, in *Seventh International Conference on Mars*, Abstract 3385, Jet Propul. Lab., Pasadena, Calif.

Garrels, R. M., and C. L. Christ (1965), *Solutions, Minerals, and Equilibria*, Harper and Row, New York.

Gellert, R., et al. (2004), Chemistry of rocks and soils in Gusev Crater from the Alpha Particle X-Ray Spectrometer, *Science*, *305*, 829–832, doi:10.1126/science.1099913.

Gellert, R., et al. (2006), Alpha Particle X-Ray Spectrometer (APXS): Results from Gusev Crater and calibration report, *J. Geophys. Res.*, *111*, E02S05, doi:10.1029/2005JE002555.

Gorevan, S. P., et al. (2003), Rock Abrasion Tool: Mars Exploration Rover mission, *J. Geophys. Res.*, *108*(E12), 8068, doi:10.1029/2003JE002061.

Greeley, R., et al. (2006), Gusev Crater: Wind-related features and processes observed by the Mars Exploration Rover Spirit, *J. Geophys. Res.*, *111*, E02S09, doi:10.1029/2005JE002491.

Grotzinger, J. P., et al. (2005), Stratigraphy, sedimentology and depositional environment of the Burns formation, Meridiani Planum, Mars, *Earth Planet. Sci. Lett.*, *240*, 11–72, doi:10.1016/j.epsl.2005.09.039.

Haberle, R. M., C. P. McKay, J. Schaeffer, N. A. Cabrol, E. A. Grin, A. P. Zent, and R. Quinn (2001), On the possibility of liquid water on present-day Mars, *J. Geophys. Res.*, *106*, 23,317–23,326, doi:10.1029/2000JE001360.

Hurowitz, J. A., S. M. McLennan, H. Y. McSween Jr., P. A. DeSouza Jr., and G. Klingelhoöfer (2006), Mixing relationships and the effects of secondary alteration in the Wishstone and Watchtower classes of Husband Hill, Gusev Crater, Mars, *J. Geophys. Res.*, *111*, E12S14, doi:10.1029/2006JE002795.

Johnson, J. W., E. H. Oelkers, and H. C. Helgeson (1992), Supcrt92: A software package for calculating the standard thermodynamic properties of minerals, gases, aqueous species and reactions from 1 to 500 bars and 0 to 1000°C, *Comput. Geosci.*, *18*, 899–947, doi:10.1016/0098-3004(92)90029-Q.

Kaufman, L., and P. J. Rousseeuw (1990), *Finding Groups in Data: An Introduction to Cluster Analysis*, Wiley-Interscience, New York.

Kolb, C., J. A. Martin-Fernandez, R. Abart, and H. Lammer (2006), The chemical variability at the surface of Mars: Implication for sediment formation and rock weathering, *Icarus*, *183*, 10–29, doi:10.1016/j.icarus.2006.01.020.

Lin, X., and W. Chameides (1991), Model studies of the impact of chemical inhomogeneity on SO_2 oxidation in warm stratiform clouds, *J. Atmos. Chem.*, *13*, 109–129, doi:10.1007/BF00115969.

Lodders, K. (1998), A survey of shergottite, nahklite and chassigny meteorites whole-rock compositions, *Meteorit. Planet. Sci.*, *33*, A183–A190.

McCollom, T. M., and B. M. Hynek (2005), A volcanic environment for bedrock diagenesis at Meridiani Planum on Mars, *Nature*, *438*, 1129–1131, doi:10.1038/nature04390.

McCoy, T. J., et al. (2007), Structure, stratigraphy, and origin of Husband Hill, Columbia Hills, Gusev Crater, Mars, *J. Geophys. Res.*, *113*, E06S03, doi:10.1029/2007JE003041.

McLennan, S. M., et al. (2005), Provenance and diagenesis of the Burns formation, Meridiani Planum, Mars, *Earth Planet. Sci. Lett.*, *240*, 95–121, doi:10.1016/j.epsl.2005.09.041.

McSween, H. Y., et al. (2006a), Characterization and petrologic interpretation of olivine-rich basalts at Gusev Crater, Mars, *J. Geophys. Res.*, *111*, E02S10, doi:10.1029/2005JE002477.

McSween, H. Y., et al. (2006b), Alkaline volcanic rocks from the Columbia Hills, Gusev Crater, Mars, *J. Geophys. Res.*, *111*, E09S91, doi:10.1029/2006JE002698.

Ming, D. W., et al. (2006), Geochemical and mineralogical indicators for aqueous processes in the Columbia Hills of Gusev Crater, Mars, *J. Geophys. Res.*, *111*, E02S12, doi:10.1029/2005JE002560.

Mittlefehldt, D. W., R. Gellert, T. J. McCoy, H. Y. McSween Jr., R. Li, and the Athena Science Team (2006), Possible Ni-rich mafic-ultramafic magmatic sequence in the Columbia Hills: Evidence from the Spirit rover, *Lunar Planet. Sci.*, *XXXVII*, Abstract 1505.

Morris, R. V., et al. (2006a), Mössbauer mineralogy of rock, soil, and dust at Gusev Crater, Mars: Spirit's journey through weakly altered olivine basalt on the plains and pervasively altered basalt in the Columbia Hills, *J. Geophys. Res.*, *111*, E02S13, doi:10.1029/2005JE002584.

Morris, R. V., et al. (2006b), Mössbauer mineralogy of rock, soil, and dust at Meridiani Planum, Mars: Opportunity's journey across sulfate-rich outcrop, basaltic sand and dust, and hematite lag deposits, *J. Geophys. Res.*, *111*, E12S15, doi:10.1029/2006JE002791.

Morris, R. V., et al. (2007), Possible evidence for iron sulfates, iron sulfides, and elemental sulfur at Gusev Crater, Mars, from MER, CRISM, and analog data, in *Seventh International Conference on Mars*, Abstract 3393, Jet Propul. Lab., Pasadena, Calif.

Murtagh, F., and A. Heck (1987), *Multivariate Data Analysis*, Kluwer Acad., Boston, Mass.

Pinet, P. C., V. V. Shevchenko, S. D. Chevrel, Y. Daydou, and C. Rosemberg (2000), Local and regional lunar regolith characteristics at Reiner Gamma Formation: Optical and spectroscopic properties from Clementine and Earth-based data, *J. Geophys. Res.*, *105*, 9457–9476, doi:10.1029/1999JE001086.

Rieder, R., R. Gellert, J. Brückner, G. Klingelhöfer, G. Dreibus, A. S. Yen, and S. W. Squyres (2003), The new Athena Alpha Particle X-Ray Spectrometer for the Mars Exploration Rovers, *J. Geophys. Res.*, *108*(E12), 8066, doi:10.1029/2003JE002150.

Rieder, R., et al. (2004), Chemistry of rocks and soils at Meridiani Planum from the Alpha Particle X-Ray Spectrometer, *Science*, *306*, 1746–1749, doi:10.1126/science.1104358.

Sievering, H., M. Keywood, R. von Glasow, M. Harvey, and J. Cainey (2006), SO_2 oxidation in seasalt aerosols: Enhanced NSS production due to biogenic alkalinity and aerosol indirect effect RF, *Eos Trans. AGU*, *87*(36), Jt. Assem. Suppl., Abstract A41H-06.

Squyres, S. W., et al. (2003), Athena Mars Rover science investigation, *J. Geophys. Res.*, *108*(E12), 8062, doi:10.1029/2003JE002121.

Squyres, S. W., et al. (2004), The Spirit Rover's Athena science investigation at Gusev Crater, Mars, *Science*, *305*, 794–799, doi:10.1126/science.3050794.

Squyres, S. W., et al. (2006a), Rocks of the Columbia Hills, *J. Geophys. Res.*, *111*, E02S11, doi:10.1029/2005JE002562.

Squyres, S. W., et al. (2006b), Overview of the Opportunity Mars Exploration Rover Mission to Meridiani Planum: Eagle Crater to Purgatory Ripple, *J. Geophys. Res.*, *111*, E12S12, doi:10.1029/2006JE002771.

Squyres, S. W., et al. (2007), Pyroclastic activity at Home Plate in Gusev Crater, Mars, *Science*, *316*, 738–742, doi:10.1126/science.1139045.

Storrie-Lombardi, M. C., and M. R. Fisk (2004), Evidence of biogenic alteration in sub-oceanic basalt glass: Complexity image analysis, elemental abundance distributions, and Bayesian probabilistic classification, in *Instruments, Methods, and Missions for Astrobiology VIII*, edited by R. B. Hoover et al., *Proc. SPIE Int. Soc. Opt. Eng.*, *5555*, 47–58.

Storrie-Lombardi, M. C., and R. B. Hoover (2004), Fossil signatures using elemental abundance distributions and Bayesian probabilistic classification, in *Instruments, Methods, and Missions for Astrobiology VIII*, edited by R. B. Hoover et al., *Proc. SPIE Int. Soc. Opt. Eng.*, *5555*, 18–30.

Tréguier, E., C. d'Uston, and R. Gellert (2006), Principal component analysis of geochemical data at Gusev Crater, *Lunar Planet. Sci.*, *XXXVII*, Abstract 1956.

Tréguier, E., C. d'Uston, O. Gasnault, P. Pinet, M. J. Toplis, R. Gellert, and the Athena Science Team (2007), Investigating geochemical relationships between Martian soils and rocks, *Lunar Planet. Sci.*, *XXXVIII*, Abstract 1730.

Van der Lee, J., and L. de Windt (2002), Chess Tutorial and Cookbook, Updated for version 3.0, *Rep. LHM/RD/02/13*, Ecole des Mines de Paris, Fontainebleau, France.

Wang, A., J. F. Bell III, R. Li, J. R. Johnson, W. Farrand, R. E. Arvidson, L. S. Crumpler, S. W. Squyres, K. Herkenhoff, A. Knudson, W. Chen, and Athena Science Team (2007), Sulfate-rich soils exposed by Spirit Rover at multiple locations in Gusev, in *Seventh International Conference on Mars*, Abstract 3348, Jet Propul. Lab., Pasadena, Calif.

Yen, A. S., et al. (2005), An integrated view of the chemistry and mineralogy of Martian soils, *Nature*, *436*, 49–54, doi:10.1038/nature03637.

Yen, A. S., et al. (2006), Nickel on Mars: Constraints on meteoritic material at the surface, *J. Geophys. Res.*, *111*, E12S11, doi:10.1029/2006JE002797.

Zolotov, M. Y., and M. V. Mironenko (2007), Timing of acid weathering on Mars: A kinetic-thermodynamic assessment, *J. Geophys. Res.*, *112*, E07006, doi:10.1029/2006JE002882.

G. Berger, Laboratoire d'étude des Mécanismes de Transfert en Géologie, OMP, CNRS, Université Paul Sabatier, 14 Avenue Edouard Belin, F-31400 Toulouse, France.

J. Brückner, Max-Planck-Institut für Chemie, Postfach 3060, D-55020 Mainz, Germany.

C. d'Uston and E. Tréguier, Centre d'Etude Spatiale des Rayonnements, OMP, CNRS, Université Paul Sabatier, 9 Avenue du Colonel Roche, F-31028 Toulouse, France. (erwan.treguier@gmail.com)

R. Gellert, Department of Physics, University of Guelph, 50 Stone Road East, Guelph, ON NIG 2W1, Canada.

T. J. McCoy, Department of Mineral Sciences, National Museum of Natural History, Smithsonian Institution, Washington, D. C. 20560-0119, USA.

P. C. Pinet and M. J. Toplis, Dynamique Terrestre et Planétaire, OMP, CNRS, Université Paul Sabatier, 14 Avenue Edouard Belin, F-31400 Toulouse, France.